



Performance of reinforced concrete slabs under punching loads

Mohamed Said · Ahmed A. Mahmoud · Ahmed Salah

Received: 28 September 2019 / Accepted: 16 June 2020 / Published online: 23 June 2020
© RILEM 2020

Abstract The experimental program of this study consisted of 12 slab specimens. The parameters investigated include ratio of reinforcement in compression and tension, amount of shear reinforcement and arrangement of shear reinforcement. Flexural reinforcement ratio especially in tension had a noticeable effect on the mode of failure and ultimate punching capacity of slabs. The enhancement in the ultimate loads due to increasing tensile reinforcement ratio was ranging between 26.0 and 42.0%. Slightly enhancement (up to 12%) in ultimate loads was observed as a result of increasing compressive steel ratio. Provision of shear reinforcement was shown to be increased the perimeter of the failure. The ultimate loads were increased with the addition of single leg stirrups as shear reinforcement particularly in case of radial arrangement of shear reinforcement. The ECCS shows the most conservative prediction for punching shear capacity specially in case of using shear reinforcement and the mean predicted-to-experimental ultimate load is shown to be 0.7. The predictions following the ACI and CSA are closet to the experimental results. The mean predicted-to-experimental ultimate load is shown to be 0.8 for ACI and 0.96 for CSA. The BS provisions for punching shear analysis were shown to be overestimated in some cases, where

the mean predicted-to-experimental ultimate load is shown to be 1.19.

Keywords Punching · Flexural reinforcement · Shear reinforcement · Energy absorption · Ductility

1 Introduction

Punching shear resistance is a major item in flat slabs design. The punching shear failure follows a mechanism that leads to the development of a failure surface in the vicinity of the supported column. The design procedures of flat slabs are governed mostly by a mode of shear failure. The shear failure occurs in the vicinity of the supporting columns is due to 2-way action of the slab. In case of the beam action, the slab behaves as a wide beam and the failure extends along the entire width of the slab near the supports [1–3].

The punching shear capacities of the tested slabs [4–6] were compared to the values predicted by the provisions of ACI 318 [7]. Predictions calculated by ACI 318 are very conservative due to the control perimeter located at 0.5d from the column face. Yang et al. [8] conducted experimental work consisted of testing six slab specimens. The objective of this investigation was discussing the influence of using high-strength steel on punching shear response of flat slabs. Replacement of conventional steel bars with

M. Said (✉) · A. A. Mahmoud · A. Salah
Civil Engineering Department, Faculty of Engineering,
Benha University, Shoubra, Cairo, Egypt
e-mail: Mohamed.abdelghaffar@feng.bu.edu.eg

high-strength steel bars, having the same area, resulted in a 27% increase of the punching shear capacity. This increasing in the punching shear resistance is due to the fact that the higher strength bars did not yield before punching failure. The steel ratio in column reign should be not less than 0.50% in the two directions with a spacing less than or equal the slab depth [9]. The cube-root relationship between punching shear capacity and the concert strength is provable than the square-root relationship used by the ACI code provision [10, 11]. The enhancement in the ultimate load was 8.5% load as the flexural reinforcement ratio increased from 0.56 to 1.28% [12].

Guandalini et al. [13] were studied the behavior of slabs with different flexural reinforcement ratios and without transverse reinforcement. For thicker slabs with low reinforcement ratios, ACI 318 is less conservative than shown in the test results. The values given by EC2 [14] provision were better correlation with the experimental results. Slabs with shear reinforcement showed noticeable increases in the shear capacity and the ductility compared with slabs without shear reinforcement [15]. Stein et al. [16] pointed out that ACI 318 code provision is satisfied to predict the punching failure capacity of specimen. The test specimens of this study showed that the flexural failure load exceeds the punching failure load by 70%.

Yaser [17] tested fifteen concrete slab specimens under the effect of line loads and concentrated loads to study the flexural and shear responses of two-way flat slabs. Slabs with small thickness and with reinforcement ratio less than 0.3% showed a real punching cracks and the punching shear failure was the governing the failure mode. The punching shear capacity increased as the slab span to slab depth ratio decreased. Marzouk et al. [18] concluded that the increased in the ultimate central deflection for specimens subjected to moment ranged between 74 and 91% for the specimens with flexural reinforcement 1.0% and 0.5% respectively. Menetrey, P. [19] tested 12 octagonal slabs to clarify the relation between flexure and punching shear behaviors. The tests revealed a transition between punching and flex-ural failure. The results indicating that increas-ing in the punching crack inclination was observed. Consequently, the sud-den decrease of the load-carrying capacity was lessened by increasing the punching crack inclination.

Kruger et al. [20] tested six flat slabs with normal strength under eccentric load. The results showed a strong effect of the load eccentricity ratio, e/t on the load carrying capacity of slab specimens. Using the shear reinforcement was increased the ultimate load capacity of the slabs by about 30-35% depending on the eccentricity ratio. ACI and CSA [7, 21] provision predicted very conservative punching strength for specimens without shear reinforcement [22].

Yamada et al. [23] studied the influence of shear reinforcement type and ratio on the punching shear behavior of slab-column joints. The failure mode of the CFRP reinforced slab column connections in punching shear was similar to that of steel reinforced connections. The crack pattern of CFRP reinforced slabs was also comparable to that of the steel reinforced slabs [24, 25]. The use of steel fiber can delay the formation of inclined shear cracks in specimens. The punching surfaces in fiber reinforced specimens were similar to those in plain concrete specimens, but with larger perimeters. The steel fiber enhanced the maximum load by about 30% to 45% [26–28].

2 Research significance

This research work is aimed to study experimentally and analytically the punching shear behavior of flat slabs. Comparisons of test results with the available analytical methods and design code equations were adopted. The study includes the effect of flexural reinforcement in both compression and tension side and the shear reinforcement on the slab behavior in punching shear. A comparison established between the experimental and the analytical results obtained from applying the punching shear strength formulae given in design codes, and the method of nonlinear finite element analysis using “ANSYS10” program.

3 Experimental program

3.1 Test specimens

The experimental program consisted of twelve half-scale slab specimens with a square shape of dimensions 1200 × 1200 mm, and with an upper column stub of 200 × 200 mm cross section and 400 mm



height. The nominal thickness of all slab specimens was 120 mm with a concrete cover of 15 mm. Typically; all test slabs were reinforced with bottom mesh and/or top mesh according to reinforcement details of test specimens. Additional shear reinforcement in the form of single leg stirrups was provided for six specimens with two manners of arrangement. Typical concrete dimensions and reinforcement details of the slab specimens are shown in Fig. 1. The experimental study investigates the influence of the selected slab parameters on the punching shear response of flat slabs. The investigated parameters include: ratio of the tensile steel, ratio of the compressive steel, amount and arrangement of the shear reinforcement.

According to Table 1, the slab specimens were classified into four groups identified A, B, C and D depending on the test parameters. Series A consists of three specimens without shear reinforcement or compressive steel and designated as S1-25, S2-25 and S3-25. The aim of this group was to evaluate the contribution of tensile steel ratio on the slab punching response. The tensile steel ratios used were 0.75%, 1.1% and 1.9%. The second group, Group B consisted of three specimens, designated as S4-25, S5-25 and S6-25, which were provided with top reinforcement with three different ratios and with bottom reinforcement ratio of 1.1%. The three ratios of compressive steel were 0.45%, 0.75% and 1.1%. This series was intended to evaluate the contribution of the compression steel to the punching shear capacity of flat slabs. Group C consisted of three specimens, designated as S7-25, S8-25 and S9-25, which were provided with shear reinforcement in the form of single leg stirrups arranged in a cross-shape in plan, as shown in Fig. 2. The stirrups used as shear reinforcement were arranged according to the ACI provisions. The distance between support face and the first line of stirrup legs should not be more than half slab thickness, and the spacing between successive lines of shear reinforcement should not be more than half slab thickness measured in a direction perpendicular to the column face. The aim of this series was to study the contribution of the stirrups to the punching shear capacity of slabs for various shear reinforcement ratios arranged in direction perpendicular to the column faces. The fourth group, Group D slabs were the same of group C but the arrangement of stirrups was taken in a radial arrangement. These specimens were

designated as S10-25, S11-25 and S12-25, as shown in Fig. 3.

The average concrete strength after 28 days was 25 MPa. Deformed high tensile steel bars of 10, 12 and 16 mm diameter with yield strength about 400 MPa and ultimate strength about 560 MPa was used. Figure 4 shows the typical test setup for tested specimens.

The deformations of test specimens were measured and monitored by LVDTs (Linear Voltage Displacement Transducers). Electrical strain gages with a gage length of 10 mm were used to measure the strains in the longitudinal bars and steel stirrups, as shown in Fig. 1b. The main components of the testing instruments are: control station, hydraulic unit, and testing frame. A schematic diagram of the test facilities is shown in Fig. 1c.

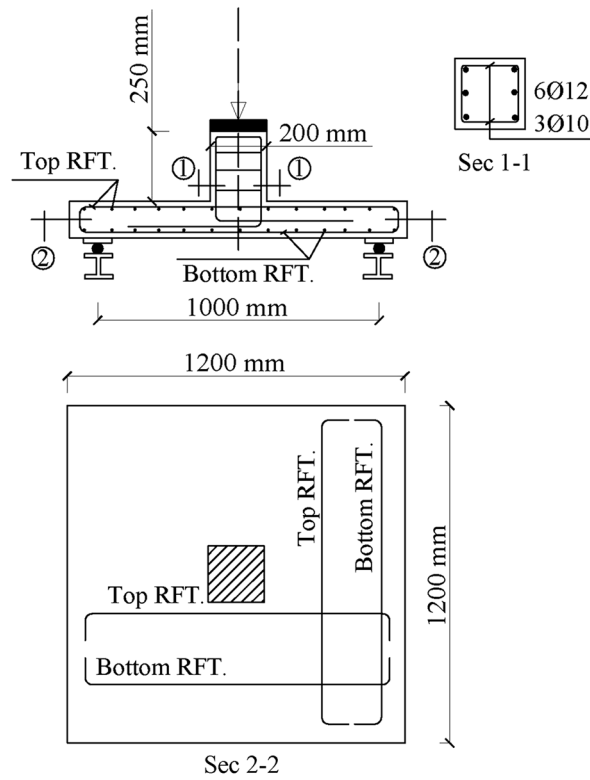
4 Results and discussion

In general, all specimens exhibited similar crack pattern before peak point. The crack pattern propagation showed very fine tangential cracks were first observed around the column stub and few fine cracks started in radial directions running from the column borders toward the slab edges. With increasing the load, the radial cracks progressed to the edges while further tangential cracks developed at greater radii. Comparable behavior was observed for specimens provided with shear reinforcement with denser crack propagation and higher failure loads. All specimens without shear reinforcement failed in a brittle sudden punching failure manner. Specimens with shear reinforcement also failed in punching mode with more ductile response. Table 1 presents the initial cracking and the ultimate loads for all specimens.

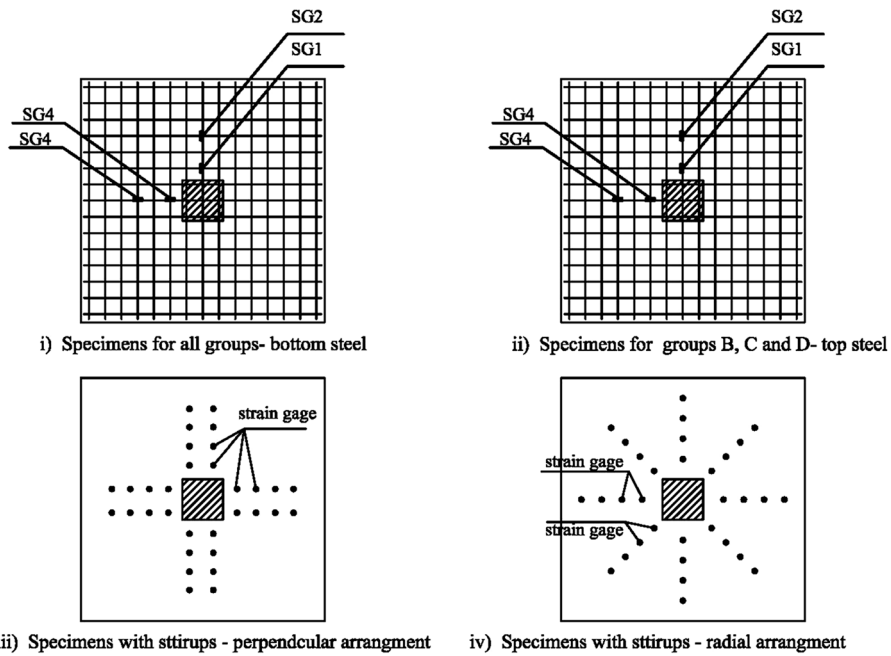
4.1 Crack pattern

4.1.1 Series (A)

For Specimen S1-25, perpendicular cracks at the column face appeared at about 75.0 KN followed by short radial and tangential cracks near the column corners at 95.0 KN. As the load increased, few radial cracks began to appear whereas the widths of the primary ones increased. The radial cracks remarkably extended at a load of 150.0 KN. At 175.0 KN, several



(a) Typical concrete dimensions and reinforcement for specimens



(b) Typical strain gauge positions for test specimens

Fig. 1 a Typical concrete dimensions and reinforcement for specimens. b Typical strain gauge positions for test specimens. c Schematic diagram of the test facilities



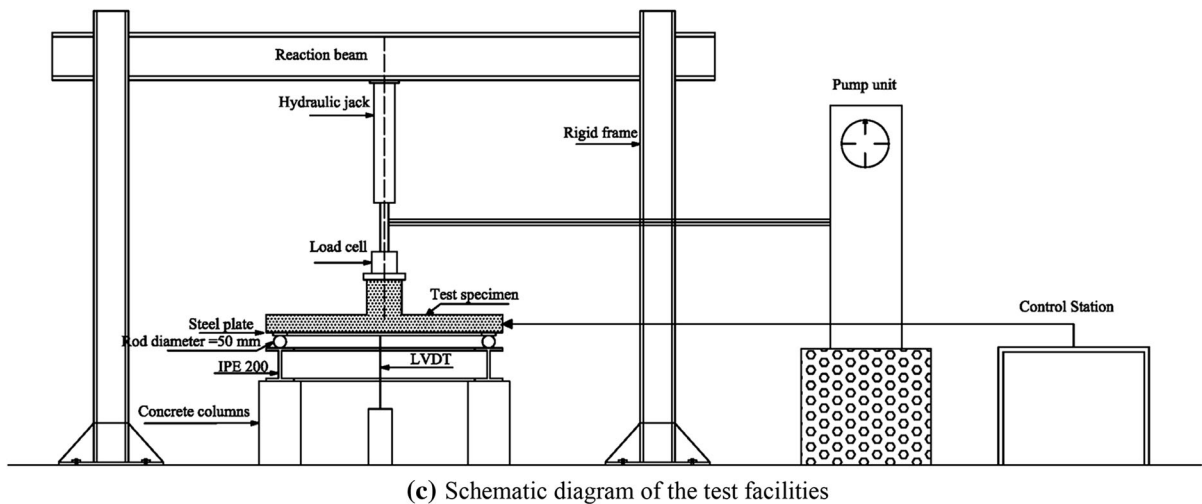


Fig. 1 continued

tangential cracks appeared around the column face. At 205.4 kN, sudden brittle failure occurred around the column with the formation of a truncated cone in the slab. At the level of the flexural reinforcement, the punching shear crack turned into a horizontal splitting following the reinforcement to the edges of the slab. At failure, the concrete cover of the bottom surface separated from the slab and few pieces of concrete fell to the ground. The cracking pattern including the failure mode of Specimen S1-25 is shown in Fig. 5a.

For Specimen S2-25, the first visible radial and tangential cracks appeared at 78.0 kN around the column. Fine tangential cracks appeared at 125.0 kN extending from the column corner making an angle of 45 degree. Development of cracking continued up to 210.0 kN. Therefore, few radial cracks formed but the width of the cracks in general continued to increase up to failure. The failure of this specimen occurred suddenly at about 259.8. The final cracking pattern of Specimen S2-25 is shown in Fig. 5b.

For Specimen S3-25, the first observed crack appeared at 97.0 kN appeared around the column at a distance of half the slab thickness. Radial cracks appeared at 135.0 kN on the bottom surface. A major tangential crack developed at a load of 220.0 kN. Propagation of radial cracks started from the column corner and began to widen very noticeably while approaching the slab support at 250.0 kN. These cracks began to join prior to the failure. This specimen failed at a load of 293.3 kN. At failure a considerable spalling of concrete cover was observed reflecting the

increased brittle nature of failure. This brittleness may be undesirable since structural failure could happen previously without noticeable cracks. Figure 5c indicates the final cracking pattern of Specimen S3-25. The ultimate load of test specimens increased as the tensile reinforcement increased. The enhancement in the ultimate loads due to increasing tensile reinforcement ratio was ranging between 26.0 and 42.0%.

4.1.2 Series (B)

Referring to Table 1, no enhancement in the first cracking load was recorded for specimens provided with top reinforcement. Series B compared to the corresponding control specimen of Series A, S2-25. Comparable cracking pattern were also observed. On the other hand, slightly enhancement in the failure load was recorded particularly for Specimen S6-25 with largest top reinforcement ratio. The enhancement in the failure loads due to using top steel was limited. The increase in the failure load was 1.0%, 9.0% and 12% for Specimens S4-25, S5-25 and S6-25, respectively compared with specimen S2-25 in series A. Failure patterns for these specimens were slightly different from that of the corresponding control specimens. The cracking patterns are shown in Fig. 6.

4.1.3 Series (C)

For Specimens S7-25, S8-25 and S9-25, the first crack appeared at 80.0 kN, 82.0 kN and 81.0 kN,

Table 1 Experimental program

Group	Specimen	Bottom RFT. ratio (%)	Top RFT. ratio (%)	Shear RFT. (mm^2)	Experimental results		Initial Stiffness; K_i (KN/mm)	Ultimate Stiffness; K_u (KN/mm)	Stiffness Degradation Ratio; K_u/K_i	Ductility Factor	Energy Absorption KN.mm	NLFEA results		NLFEA/EXP.	
					Initial cracking load, V_{CT} (KN)	Failure load, V_{EXP} (KN)						Cracking load V_{CA} (KN)	Ultimate load V_{FA} (KN)		V_{CA}/V_{CT}
A	S1-25	0.75	-	-	75.0	205.4	17.1	13.7	0.80	1.31	832.3	64.0	224.0	0.85	1.09
	S2-25	1.10	-	-	78.0	259.8	27.6	23.3	0.85	1.37	839.6	66.0	284.0	0.84	1.09
	S3-25	1.90	-	-	97.0	293.3	35.9	31.6	0.88	1.51	825.8	70.0	314.0	0.72	1.07
B	S4-25	1.10	0.45	-	81.0	262.5	33.7	26.8	0.79	1.50	986.3	66.0	264.0	0.81	1.01
	S5-25	1.10	0.75	-	79.0	282.2	35.3	28.4	0.80	1.59	1059.9	66.0	280.0	0.83	0.99
	S6-25	1.10	1.10	-	76.0	290.9	36.8	29.2	0.79	1.71	1046.5	66.0	292.0	0.86	1.01
C	S7-25	1.10	0.75	400	80.0	299.3	35.7	29.9	0.84	2.2	1450.9	66.0	335.0	0.82	1.12
	S8-25	1.10	0.75	624	82.0	325.8	35.2	28.7	0.81	2.65	1984.3	66.0	350.0	0.80	1.07
	S9-25	1.10	0.75	904	81.0	344.7	36.1	30.1	0.83	3.64	2116.5	66.00	360.0	0.81	1.04
D	S10-25	1.10	0.75	400	82.0	305.2	34.2	30.2	0.83	1.85	1842.6	66.0	350.0	0.80	1.15
	S11-25	1.10	0.75	624	83.0	338.8	36.9	29.9	0.81	2.62	2311.3	66.0	360.0	0.79	1.06
	S12-25	1.10	0.75	904	79.0	359.3	37.4	31.7	0.84	3.51	2898.2	66.0	370.0	0.83	1.03



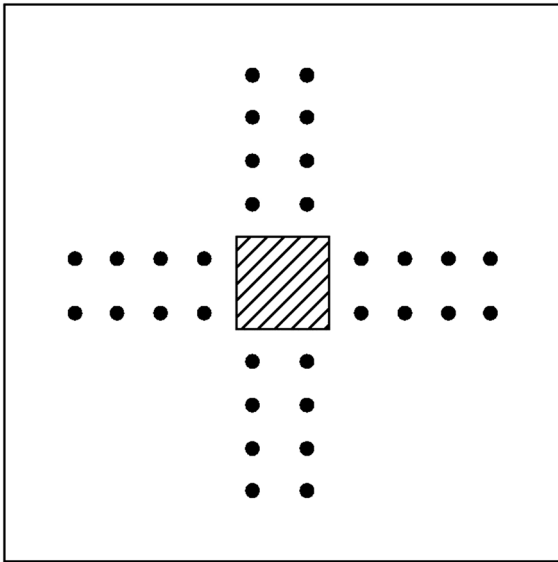


Fig. 2 Arrangement of shear link for specimens (Group C)

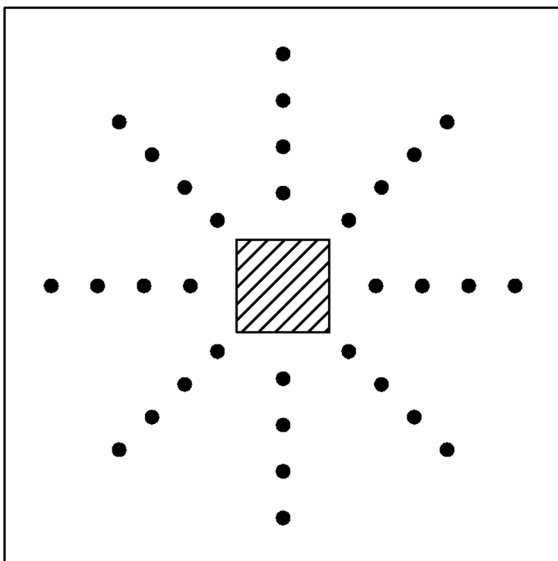


Fig. 3 Arrangement of shear link for specimens (Group D)

respectively. The first crack was independent on the shear reinforcement. The cracking patterns of these specimens were similar to those of the corresponding control specimen of Series B, S5-25. However, the cracking density was higher for the specimens of Series C. In general, the cracking and failure responses of these specimens reveal the benefits of shear reinforcement. The enhancement in the failure load



Fig. 4 Test setup

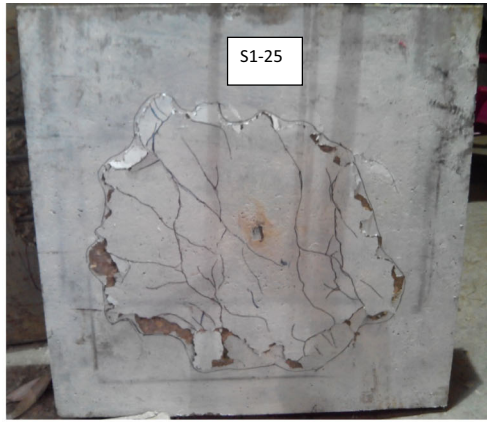
was 6.0%, 15.0% and 22.0% for Specimens S7-25, S8-25 and S9-25, respectively. The insignificant enhancement attained for Specimen S7-25 was attributed mainly to the relatively low shear reinforcement ratio. Compared to specimens of Series B, the failure surfaces had wider perimeters. The results of Series C were matching with the provisions of the ACI Code. Figure 7 show the cracking patterns of these specimens.

4.1.4 Series (D)

The overall behavior observed for test specimens provided with shear reinforcement was comparable for all specimens of Series C and series D. Of a particular interest, the crack patterns were similar with some concentration of cracking around the column region. The radial cracks were started at the column corner. Many cracks initiated on the compression face of the slabs at approximately 85% of the ultimate load. Near failure, wide and dense propagation was shown for tangential and radial cracks. The failure loads for Specimens S10-25, S11-25 and S12-25 were 305.2 KN, 338.8 KN and 359.3 KN representing increasing in the load-carrying capacity of 8.0%, 20.0% and 27.0%, respectively. The crack patterns of these specimens were shown in Fig. 8. The cracking loads of these specimens were comparable to the cracking loads of other specimens.

4.2 Effect of test parameters on cracks pattern and failure modes

The cracks patterns of specimens without shear reinforcement or top reinforcement (Series A) were



(a) Specimen S1-25



(a) Specimen S4-25



(b) Specimen S2-25



(b) Specimen S5-25



(c) Specimen S3-25



(c) Specimen S6-25

Fig. 5 Cracks pattern and failure surface of Series A

Fig. 6 Cracks pattern and failure surface of Series B

comparable. The effect of the tensile reinforcement was insignificant on the crack pattern. Specimens with top and bottom reinforcement (Series B), the cracking

patterns were quite similar to those of specimens without top reinforcement. The cracks patterns of

specimens of Series C and Series D were also comparable to the other specimens. The cracks of these specimens were more closely spaced and propagated in wider area on the bottom surface of the slab. Moreover, visual inspections indicated that the crack width slightly decreased in case of using shear reinforcement. The specimens reinforced in shear exhibited larger perimeters of punching. The radii of the punching surfaces for specimens without shear reinforcement (S4-25, S5-25 and S6-25) were approximately 250 mm at the bottom face of the slab, while for Specimens S7-25, S8-25 and S9-25 were 300, 350 and 400 mm, respectively. For specimens S10-25, S11-25 and S12-25 the radii of the punching surfaces were 325, 400 and 425 mm, respectively. The test results of Series C and D pointed out that the significance of the shear reinforcement.

In general, the failure of all test specimens was characterized by a noticeable drop in the sustained load and a large increase in the vertical displacement of the slab specimen. The final failure was accompanied by extensive and wide cracks and by visible movement of the truncated concrete cone surrounding the column. Spalling of the concrete cover in the most stressed region of the slab in shear was observed in specimens provided with shear reinforcement. At the reinforcement level, the shear crack turned into a horizontal crack parallel to the reinforcement extending to the edges of the slab. This implies that the reinforcement layer had induced a horizontal splitting of the concrete. However, this was not likely to be the cause of failure. The test specimens without shear reinforcement (Series A and Series B) failed in a brittle manner with a sudden loss in load capacity. The use of shear reinforcement (Series C and Series D) resulted in less brittle failure. Specimens of Series D had failure surfaces formed outside the shear reinforcement region.

4.3 Load deflection behaviour

The load-central deflection curves of the test specimens are plotted for each series of specimens in Fig. 9. Referring to Fig. 9, the pre-peak load–deflection relationships are shown to be comparable with almost linear response up to the peak load, irrespective of test parameters investigated. The pre-cracking behaviors for all specimens are quite similar. The post-peak load response of the specimens provided with shear

reinforcement exhibited a long plateau, Fig. 9. These specimens featured ample warning near failure.

Figure 9a shows the effect of the tensile reinforcement ratio on the overall response of the control slabs (Series A). As shown, increasing in the tensile reinforcement ratio had a significant effect on the slab stiffness. The slopes of the curves are shown to be less steeper as the tensile reinforcement ratio increased after cracking stages up to failure. The influence of cracking on the load–deflection response was similar being independent on the tensile reinforcement ratio. The maximum deflection was shown to be decreased with increasing the tensile reinforcement ratio. The decreased in deflection was about 20% and 31% for a tensile reinforcement ratio 1.10% and 1.90%, respectively. For Series A, the tensile reinforcement ratio had no influence on the post peak behavior. The enhancement in the failure loads for specimens reinforced with tensile steel only was ranging between 26.0 and 42.0%, while the ratio of tensile steel increased from 0.75 to 1.1% and 1.9%. Several researchers such as [9, 15, 28–30] also investigated the increases in the punching load carrying capacity with the increase of flexural reinforcement of slab.

The load–deflection behavior for specimens with compressive reinforcement was shown in Figs. 9b. Obviously, the effect of compressive reinforcement was remarkable especially on post-peak behavior. The pre-cracking behavior was similar to that for specimen without compressive reinforcement indicating that the compressive reinforcement had no effect on the initial stiffness. The post-peak behavior was quite similar, except in specimen S6-25 which characterized by the long plateau developed after the peak load. The maximum deflection was shown to be increased with increasing the compressive reinforcement ratio. The increase in deflection was about 7.0% and 10.0% for a compressive reinforcement ratio 0.75% m and 1.10%, respectively. The enhancement due compressive steel was 1.0%, 9.0% and 12.0% for Specimens S4-25, S5-25 and S6-25, respectively compared to Specimen S2-25, which has no compressive steel and with the same tensile steel ratio.

The load–deflection responses for specimens with shear reinforcement were shown in Fig. 9c and d. The effect of shear reinforcement was remarkable especially on post-peak behavior. The pre-cracking behavior was similar to that for specimen without shear reinforcement indicating that the shear reinforcement



(a) Specimen S7-25



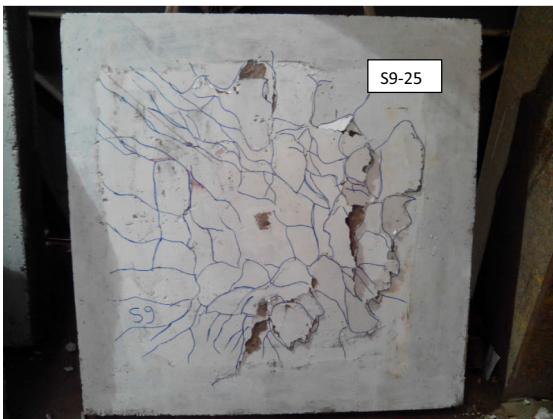
(a) Specimen S10-25



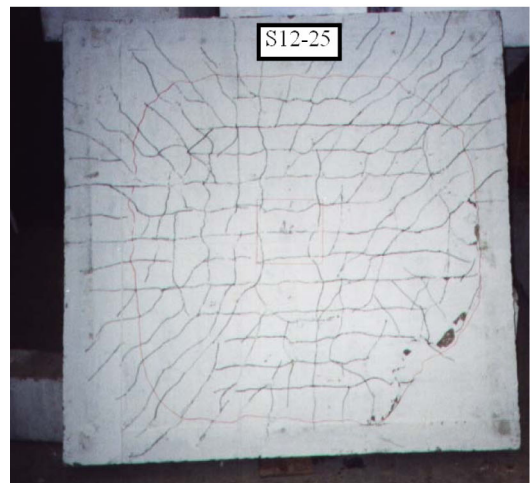
(b) Specimen S8-25



(b) Specimen S11-25



(c) Specimen S9-25



(c) Specimen S12-25

Fig. 7 Cracks pattern and failure surface of Series C

had no effect on the initial stiffness. The post-peak behavior was ductile, being characterized by the long plateau developed after the peak load. The maximum

◀ **Fig. 8** Cracks pattern and failure surface of Series D

deflection was shown to be increased with increasing the shear reinforcement ratio. The increasing in deflection in Series C was about 20.0% and 31.0% for specimen S8-25 and S9-25, respectively. Also, the increase in deflection in Series D was about 8.0% and 39.0% for Specimen S11-25 and S12-25, respectively. Provision of shear reinforcement increased the efficiency of slab column connection by a noticeable enhancement in ultimate load results and the ductility response of slab specimens. The enhancement in failure loads for this Series C was 6.0%, 15.0% and 22.0% for Specimens S7-25, S8-25 and S9-25, respectively compared to Specimen S4-25, which considered the control specimen. Limited enhancement in the ultimate capacity was observed for Specimen S7-25 reinforced mild steel and lower ratio of shear reinforcement. The enhancement in failure loads achieved in Specimens S10-25, S11-25 and S12-25 was 8.0%, 20.0% and 27.0%, respectively

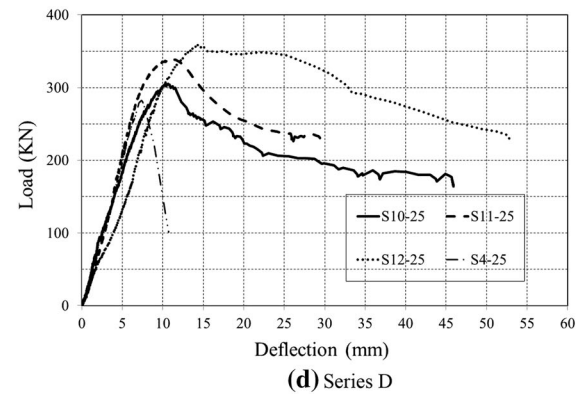
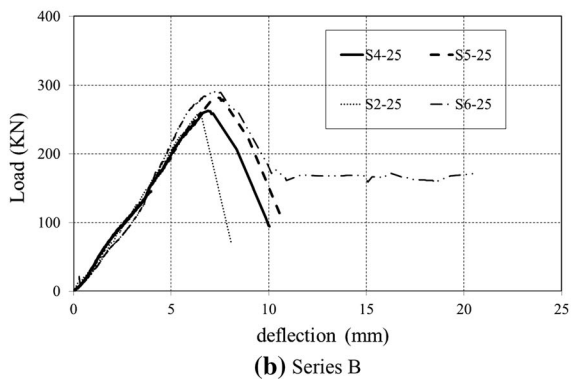
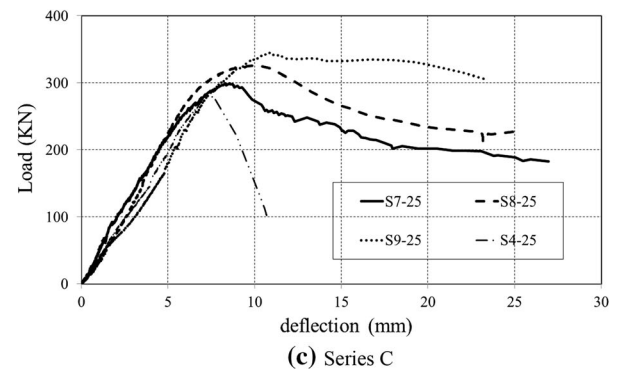
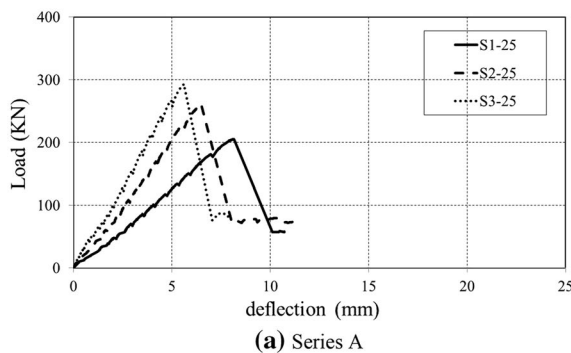


Fig. 9 Load deflection relationship for specimens

compared to Specimen S4-25, which considered the control specimen. Observation recorded by Kruger et al. [20] adopted a maximum increasing in ultimate failure load up to 35.0% in case of using U-shaped stirrups as shear reinforcement of 10 mm diameter distributed around the column to a distance of 1.0 m (8d). The footings provided with shear reinforcement had about 35% to 55% higher punching shear strengths than the corresponding footings without shear reinforcement [31].

4.4 Strains in flexural and shear reinforcement

Figure 10 shows the steel strain distribution in the bottom bar close to the centerline of the column section and parallel to the plane of bending, for the tested specimens near failure. As shown, the strain distribution is similar for all specimens. Steel strain in tensile reinforcement is shown to be under yield point until peak load for all specimens in specimen of Series A and B. This result indicated that, all test specimens failed in punching mode. For specimens in Series C

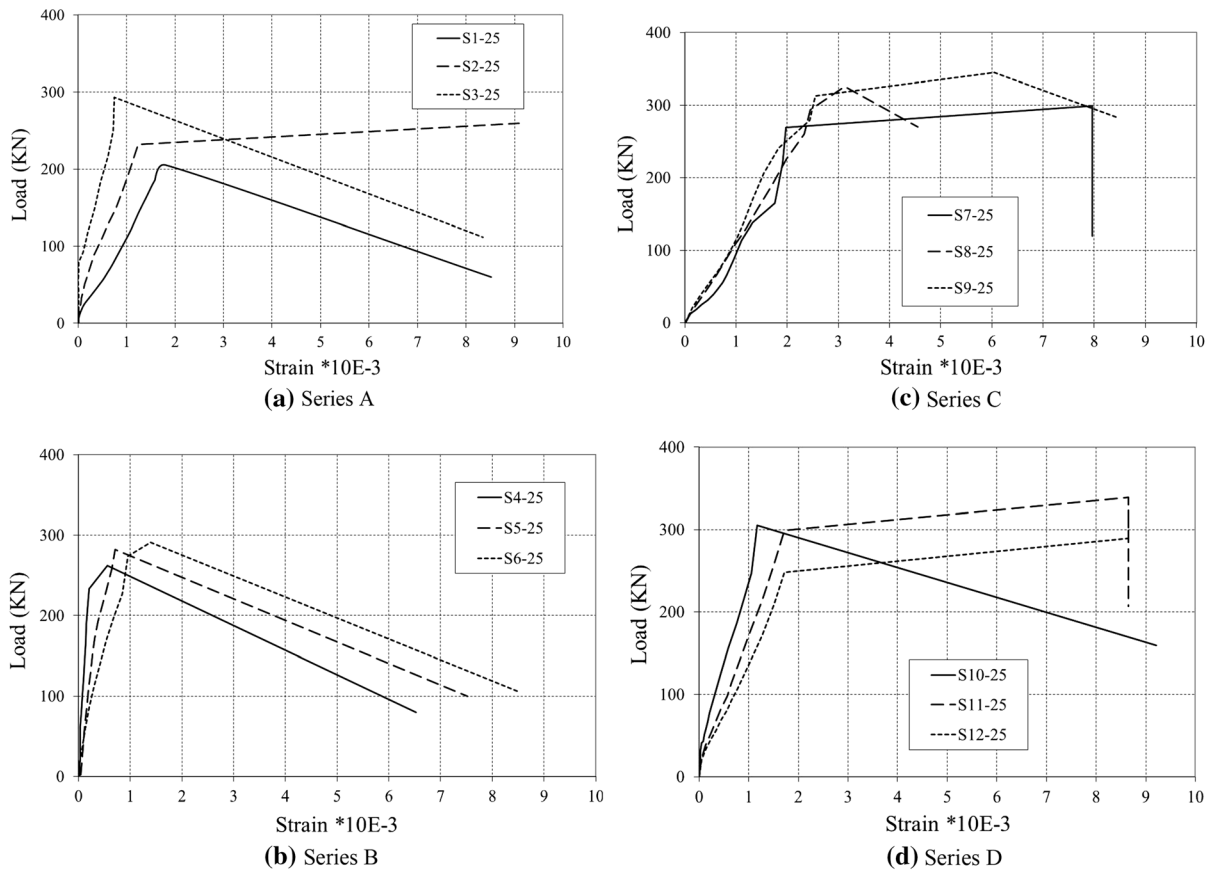


Fig. 10 Steel strain in bottom steel bars

and D the strain in the bottom reinforcement yielded just before the failure confirming the more ductile mode of failure observed in tests. Furthermore, the steel strain in specimens with shear reinforcement at a specific load level was less than that for specimens without shear reinforcement.

Figure 11 shows the steel strain distribution in the top bar close to the centerline of the column section and parallel to the plane of bending in Series B. The strain distribution is similar for all specimens characterized by low levels of strain values in the beginning of loading increasing slowly while the load increasing up to peak load. These results indicating that, the slight effect of compression steel reinforcement on punching shear capacity.

The strain in shear reinforcement was measured at the critical punching surface in order to evaluate its effectiveness. Figure 12a shows the strain variation for single leg stirrups used as shear reinforcement in Series C. As shown, the strains in the stirrups confirm

the effectiveness of this type of shear reinforcement in enhancing the punching shear capacity of test specimens. The strain in Specimen S10-25 reached the yield value at 80% of the ultimate load. Comparable conduct was observed for specimens in series D, Fig. 12b. The strain in stirrups of specimens appeared to be affected by nearby formation of some inclined cracks. The specimens with shear reinforcement in general failed by punching at the borderline between being within and being outside the shear reinforcement region.

4.5 Stiffness

According to Marzouk and Hussein [11], the stiffness of test specimens can be assessed. Initial stiffness, K_i is defined as the initial slope of load–deflection curve and ultimate stiffness, K_u is the slope of load–deflection curve at 90% of peak load. Thus, the stiffness degradation was taken as the ratio between

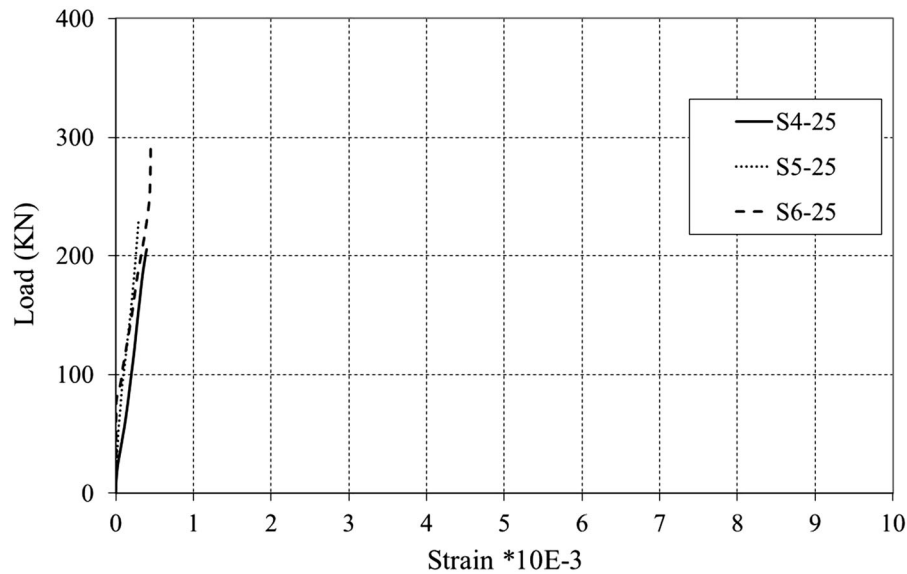


Fig. 11 Steel strain in top steel bars

the ultimate stiffness and initial stiffness, K_u/K_i . The ratio of the tensile reinforcement had a noticeable effect on the initial and ultimate stiffness. The initial and ultimate stiffness increased as the tensile reinforcement increased. The increased in the initial stiffness in series (A) was 60% and 100% for specimens S2-25 and S3-25, respectively. Also, the increased of the ultimate stiffness in series (A) was 70% and 95% for specimens S2-25 and S3-25, respectively. The stiffness degradation ratio slightly increased as the tensile reinforcement ratio increased. The increased in stiffness degradation ratio in Series (A) was about 6% and 12% for Specimens S2-25 and S3-25. The direct effect of the shear reinforcement on the initial and ultimate stiffness was not clear. The presence of top reinforcement had insignificant effect on initial stiffness and ultimate stiffness.

4.6 Ductility and energy absorption

The ductility factor, μ may be defined as the ratio of the ultimate deflection (at 80% of the peak load on the descending part of the load deflection curve) to the deflection at the beginning of the horizontal path (at 80% of the ultimate load on the ascending branch of the load deflection curve) [32]. The energy absorption is defined as the area under the load–deflection curve up to ultimate load [32]. Table 1 shows the ductility factor for all test specimens. The ductility factor for

Series (A) slabs increase by about 10% and 15% for specimens S2-25 and S3-25, respectively as the tensile steel ratio increased. The presence of shear reinforcement resulted in increases in the ductility by about 30% to 90%. Insignificant effect of the top reinforcement ratio on the slab ductility was observed.

The energy absorption is defined as the area under the load–deflection curve up to maximum load. Table 1 shows that, the energy absorbed by deflection, in general, not influenced as the tensile or compressive steel ratios increased. Referring to Series (A) results, the energy absorbed for Specimens S1-25, S2-25 and S3-25 was 832.3, 839.6 and 825.8, respectively. The presence of single leg stirrups in perpendicular arrangement increased the energy absorbed from 36 to 45% for specimens of series C. For specimens provided with single leg stirrups arranged in radial direction, the increased in the absorbed energy was 25% and 56% for specimens of series D.

4.7 Non-linear finite element analysis

The nonlinear finite element analysis was adopted using “ANSYS 10.0” computer program. A correlative study based on the load–deflection behavior was established to verify the analytical model with the experimental results. Therefore, correlating the load–deflection relationship of the analytical results with the experimental ones is considered an effective method

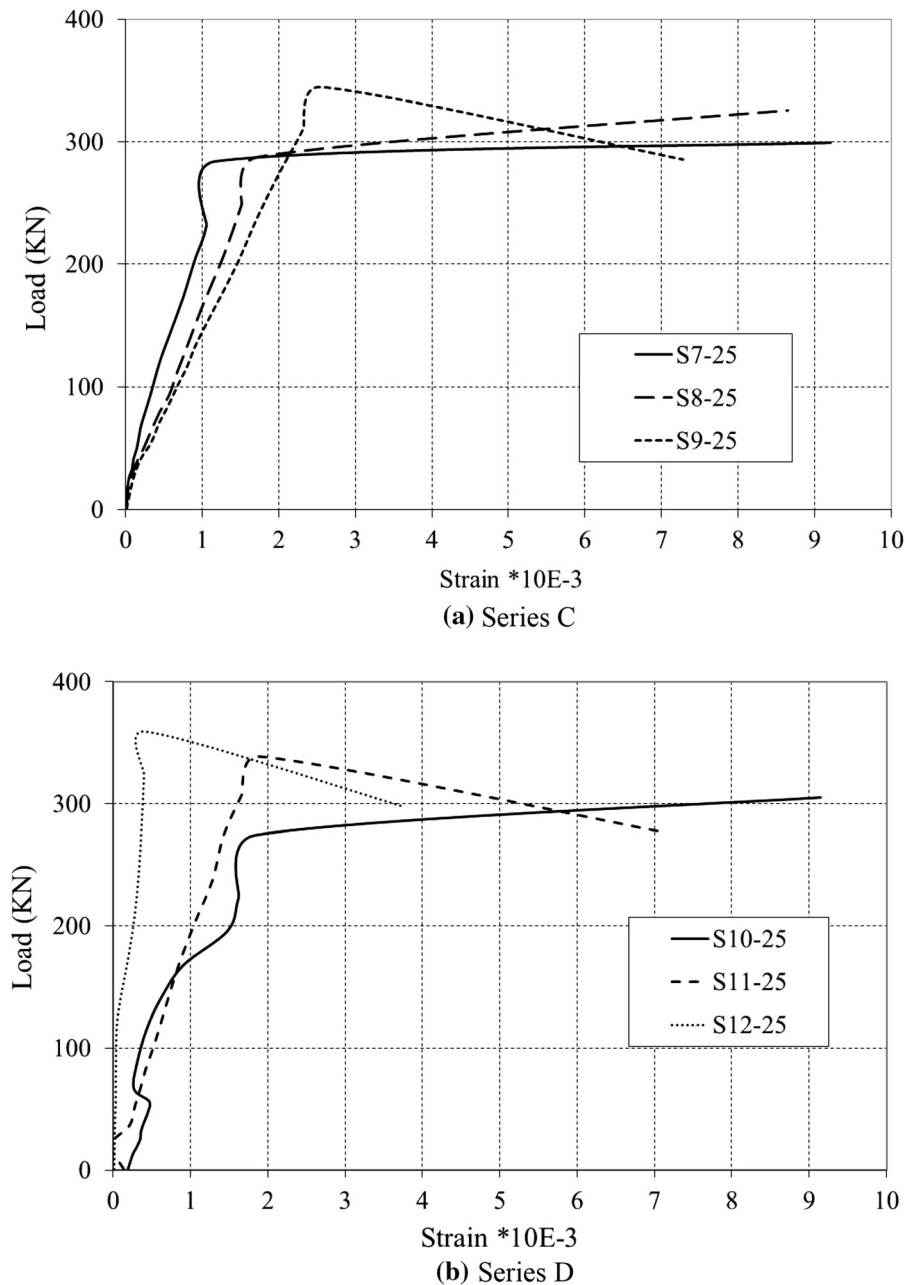


Fig. 12 Strain in shear reinforcement for Series C and D

to verify the non-linear model. Tested slabs were typically discretized using 24x24x5 mesh of nearly equal-size 3-D isoparametric elements, Solid65 as shown in Fig. 13. Five elements were used to idealize the slab thickness. The top and bottom element represent the top and bottom concert cover and the in between three elements accounted the slab

thickness. The column stub was represented as shown in the figure to simulate the actual shape and dimensions of column stub of the test specimens. The slabs were analyzed as simply supported along the four sides to simulate the experimental set-up. Referring to ANSYS technical manual, the three-dimensional isoparametric element Solid65 was adopted to

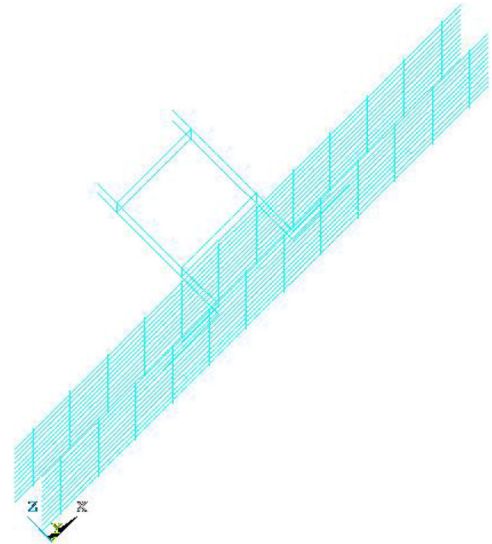
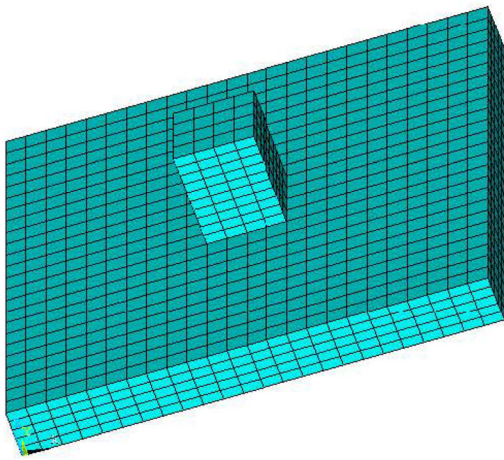


Fig. 13 Typical idealization of test slab

model the concrete element. The Solid65 element is capable of cracking in tension and crushing in compression. This element is similar to the one recommended by H.M. Marzouk (11), who introduced a three-dimensional, 8-node isoparametric element. The reinforcing bars were idealized using a 2-node bar (linear) element (Link8).

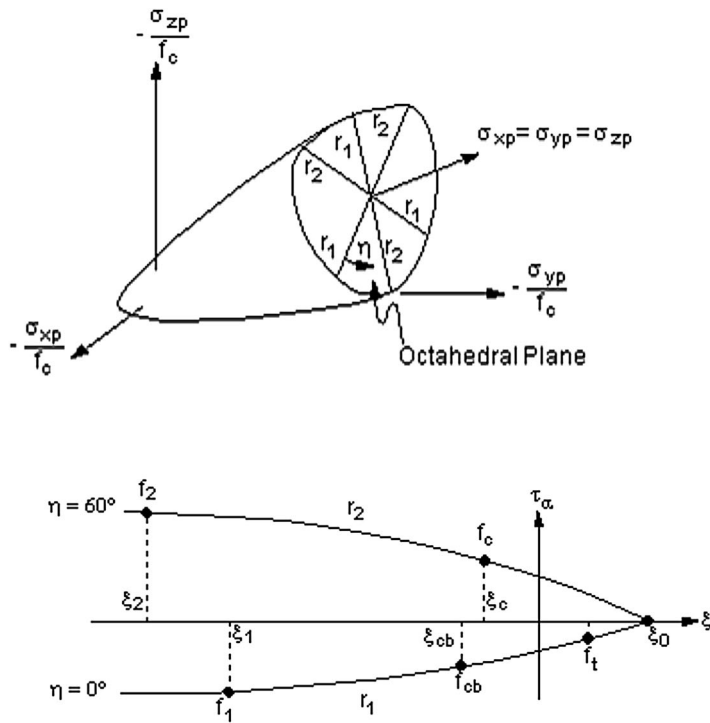
The concrete material model is characterized by its capability to predict the failure of brittle materials. Both cracking and crushing failure modes are included. The failure surface is shown as 3-D failure surface in principal stress space, Fig. 14. The angle of similarity η describes the relative magnitudes of the principal stresses. Failure surface in principal stress space with nearly biaxial stress represents the 3-D failure surface for states of stress that are biaxial or nearly biaxial, Figs. 5, 4. If the most significant non-zero principal stresses are in the σ_{xp} and σ_{yp} directions, the three surfaces presented are for σ_{zp} slightly greater than zero, σ_{zp} equal to zero, and σ_{zp} slightly less than zero. Although the three surfaces, shown as projections on the σ_{xp} - σ_{yp} plane, are nearly equivalent and the 3-D failure surface is continuous, the mode of material failure is a function of the sign of σ_{zp} . For example, if σ_{xp} and σ_{yp} are both negative and σ_{zp} is slightly positive, cracking would be predicted in a direction perpendicular to the σ_{zp} direction. However, if σ_{zp} is zero or slightly negative, the material is assumed to crush.

Input strength parameters f_t (tensile strength of concrete), f_c (compressive strength of concrete), f_{cb} (Ultimate biaxial compressive strength), f_1 (Ultimate compressive strength for a state of biaxial compression superimposed on hydrostatic stress state) and f_2 (Ultimate compressive strength for a state of uniaxial compression superimposed on hydrostatic stress state) are needed to define the failure surface as well as a tri-axial stress state. The ultimate uniaxial compressive strength f_c , was taken based on test results of cylindrical and cube concrete samples for each slab specimens, and f_t was taken as recommended by ACI specifications, ($f_t = 0.1 f_c$). The other parameters were taken with recommended default values

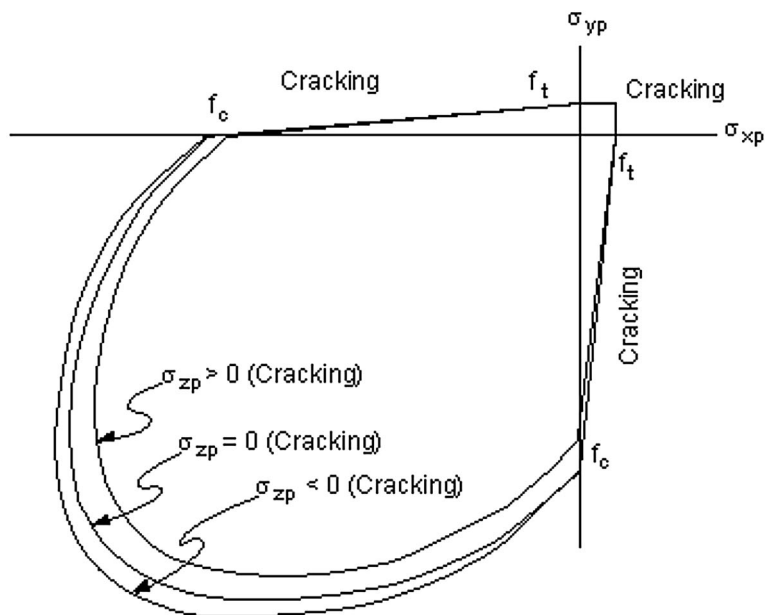
$$f_{cb} = 1.2 f_c, f_1 = 1.45 f_c, \text{ and } f_2 = 1.725 f_c$$

Additional concrete material data, such as the shear transfer coefficient in case of closed and open crack, tensile stress, and compressive stress are also required. Typical shear transfer coefficient ranges from 0.0 to 1.0, with zero-value representing a very smooth crack (complete loss of shear transfer) and 1.0 representing a very rough crack (no loss of shear transfer). This feature may be applied for both the open and closed crack. Shear transfer coefficients were taken as 0.2 for open crack and 0.8 for closed crack.

Outputs for NLFEA are shown in Table 1 and Figs. 15, 16. Respectively, these figures indicate the cracks propagation and slab concrete stresses. As

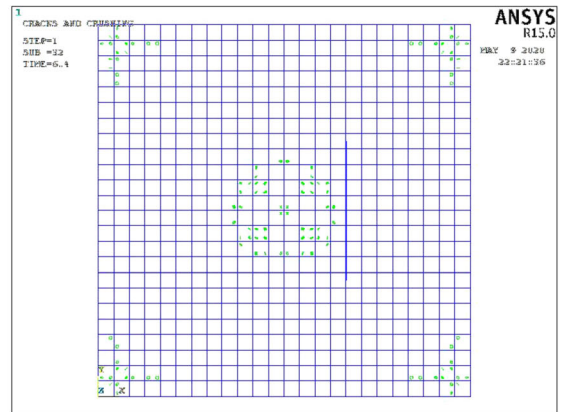
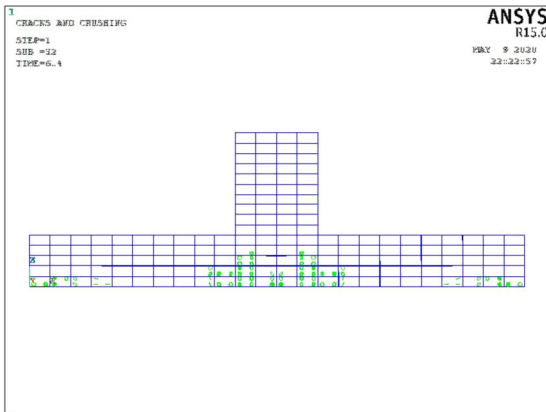


(a) 3-D Failure Surface of concrete material and its Profile.

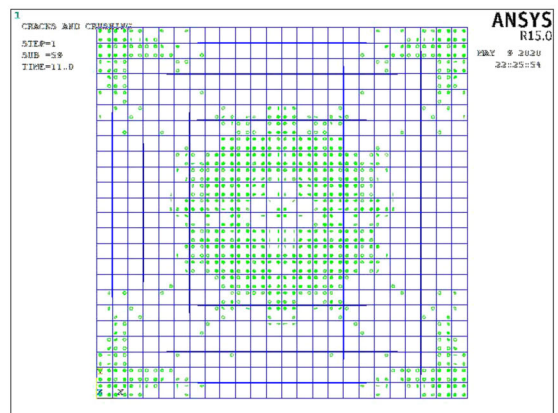
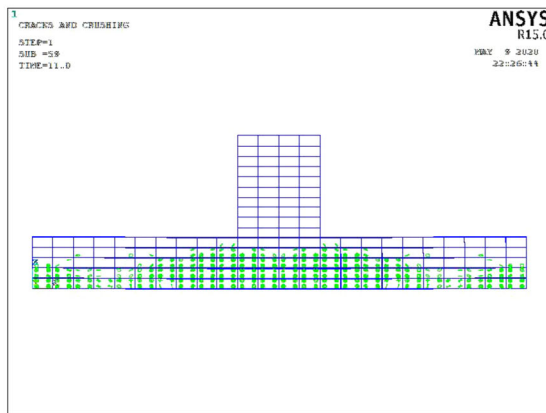


(b) Concrete material failure surface in principal stress space with biaxial stress

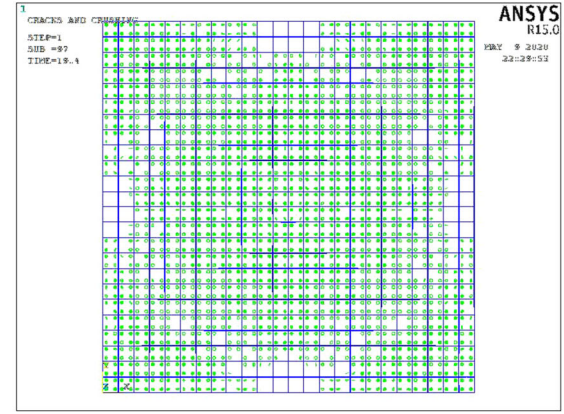
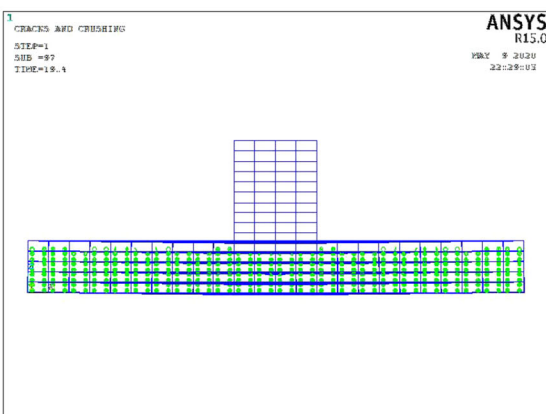
Fig. 14 a 3-D Failure Surface of concrete material and its Profile. b Concrete material failure surface in principal stress space with biaxial stress



(a) 30% V_{FA} .



(b) 60% V_{FA} .

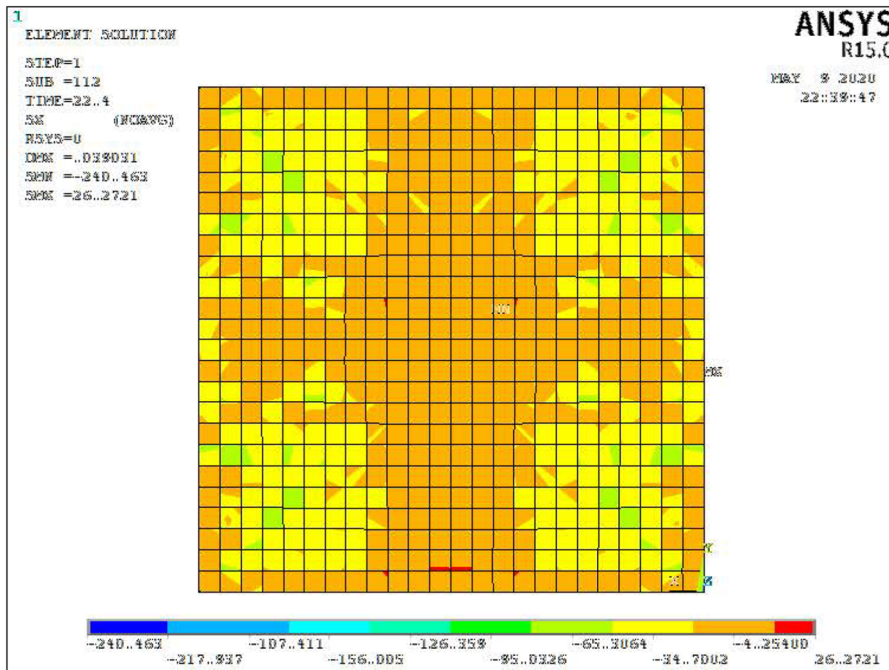


(c) 90% V_{FA} .

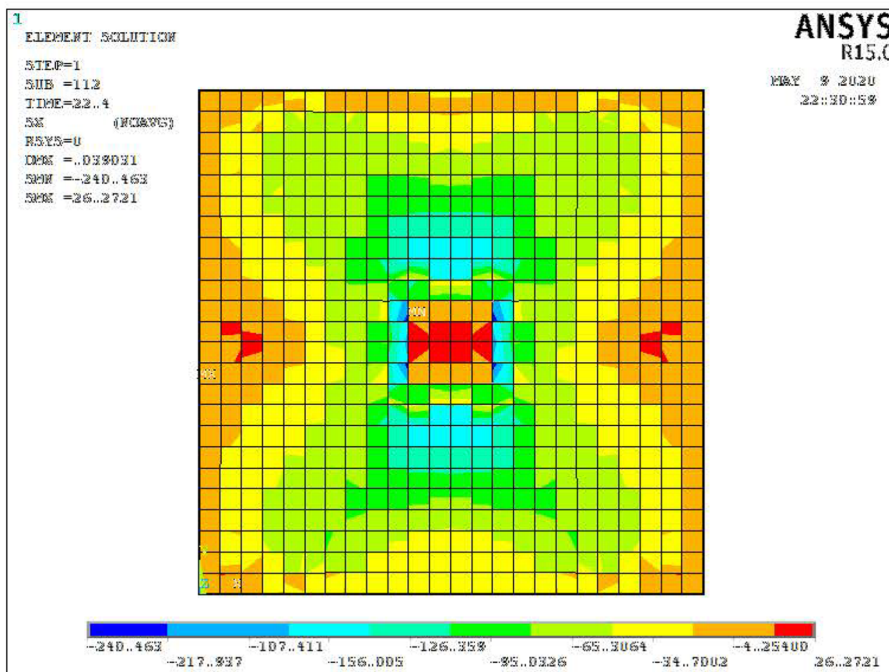
Fig. 15 Cracks propagation for Specimen S1-25

shown, following of the cracks formation shows initiation of the radial cracks from the column corners.

These cracks followed by formation of some tangential cracks. Increasing load levels the radial cracks



(a) Slab bottom surface.



(b) Slab top surface.

Fig. 16 Concrete stresses for Specimen S1-25 at failure (in Kg/cm²)

propagate towards the slab corners and the tangential cracks spread at larger perimeters, agreeing with

experimental observations. The analytical concrete stresses reveal the splitting mode of punching failure



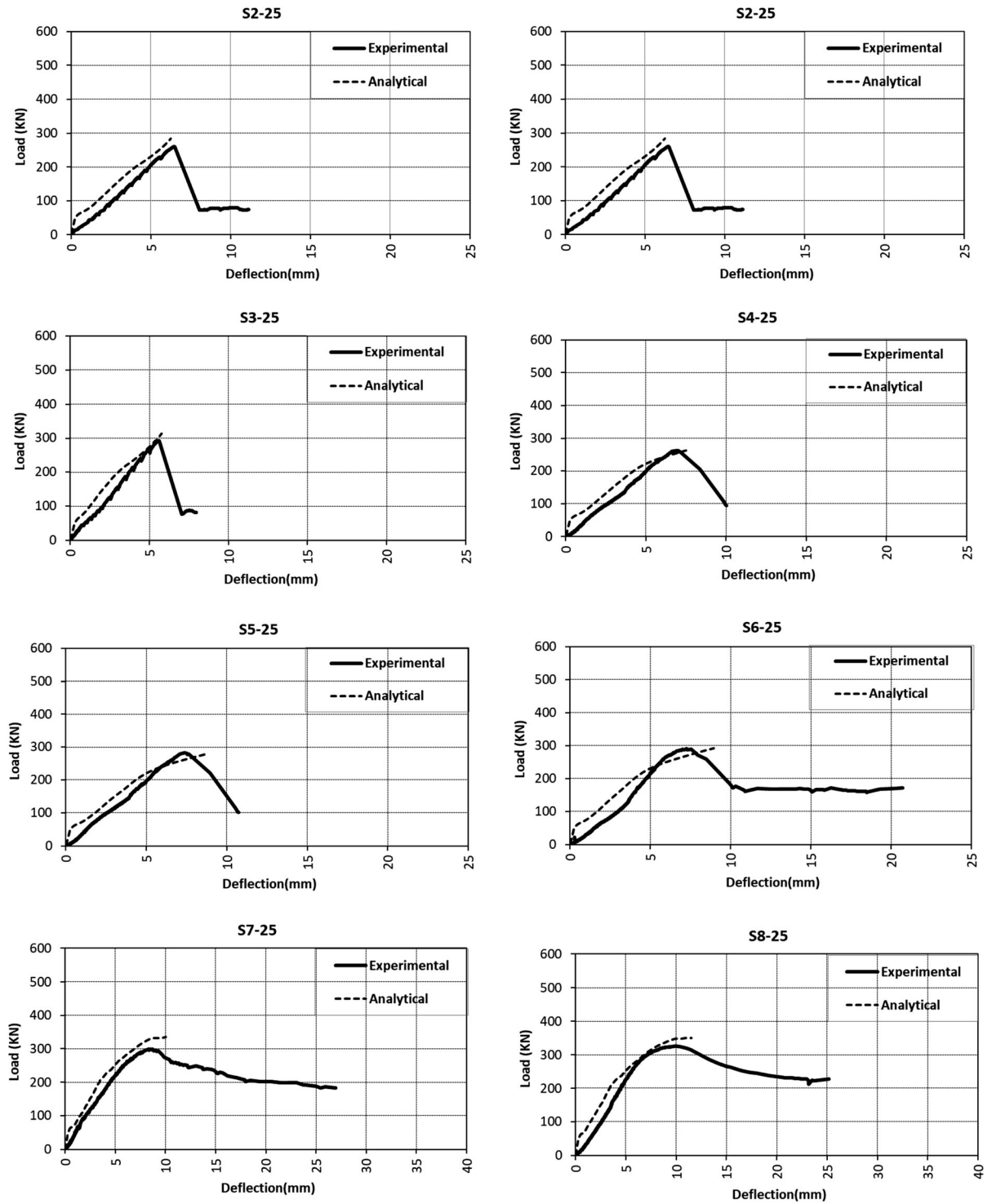


Fig. 17 Experimental and analytical load- deflection relationship for test specimens

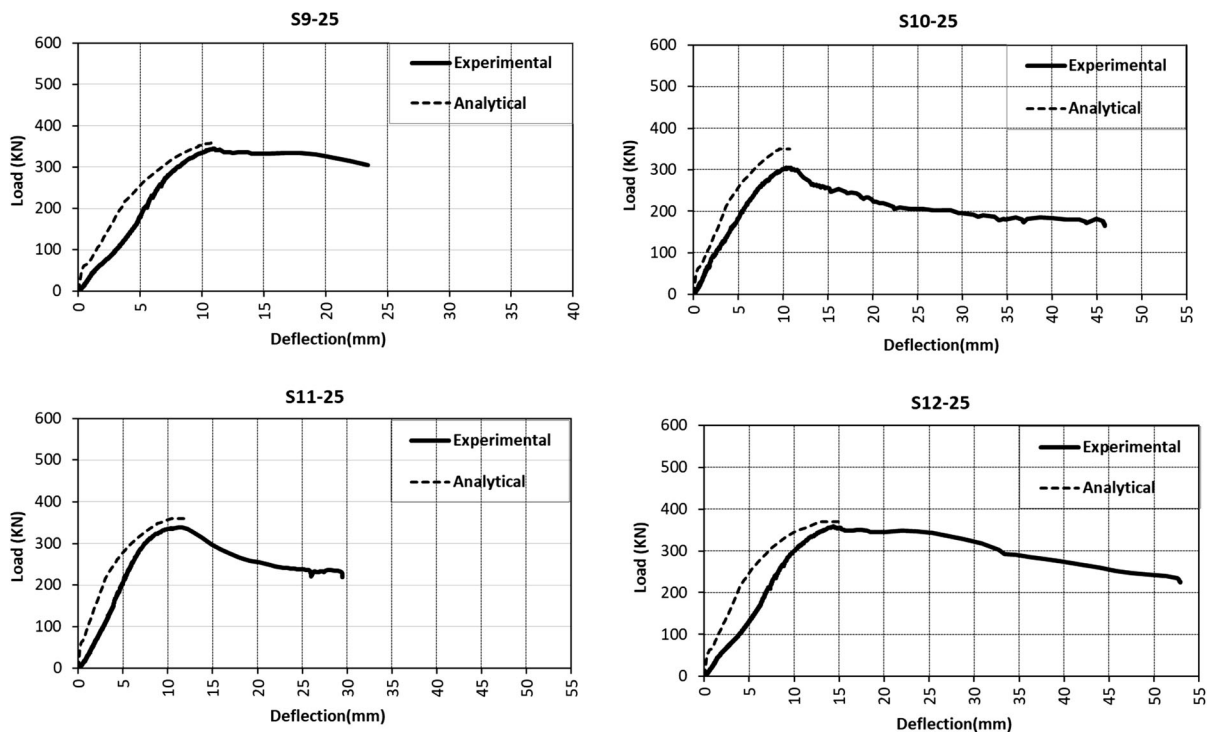


Fig. 17 continued

obtained for this specimen. The maximum analytical compressive stress for concrete was 24.0 MPa at top surface.

Referring to Fig. 17, NLFEA good estimation of the central deflection throughout the loading stages for most of the test specimens was achieved. Also, the analysis failed to predict the post-peak behavior for some test slab specimens especially those undergo sudden punching failure. Slopes of load deflection relationship by NLFEA mostly shown to be slightly steeper than experimental results.

On the other hand, results obtained from the NLFEA reflected the trend of the experimental ultimate load and maximum central deflection results. In conclusion, to the range of the test parameters investigated, the application of non-linear finite element analysis using ANSYS 10 package yielded satisfactory load-carrying capacities, and acceptable cracking capacities and load–deflection response.

Referring to Table 1, the predicted cracking loads; V_{CA} are in general less than the experimental loads; V_{CT} with a mean V_{CA}/V_{CT} ratio of 0.81. The concrete cracking strength used in the NLFEA which according to ACI provisions might be underestimated or may be

invisible cracks was produced in specimen. The cracking strength of concrete was taken as 10% of the concrete compressive strength. Specifically, underestimated predictions for the cracking loads were obtained for specimens of Series A, where the mean V_{CA}/V_{CT} ratio was 0.8 For specimens of Series B, quite nearly estimation of the cracking loads was shown in Table 1. The mean ratio V_{CA}/V_{CT} was 0.83 Conservative predictions were attained for specimens provided with shear reinforcement, with a mean V_{CA}/V_{CT} of 0.80 and. The ratio between the analytical and experimental ultimate loads; V_{FA}/V_{EXP} is indicated in Table 1, the ratio ranged between 0.99 and 1.15, with a mean value of 1.06. Individually, the mean V_{FA}/V_{EXP} ratio for specimens without shear reinforcement was 1.04. For specimens with shear reinforcement, the mean V_{FA}/V_{EXP} ratio for specimens without shear reinforcement was 1.08.

4.8 Building codes predictions

The design equations for punching shear strength incorporated in the various code provisions were essentially follow the empirical procedures derived

Table 2 Comparison of test results with the predictions of building codes

Specimen	Experimental ultimate load; VEXP (KN)	Predicted ultimate load; V (KN)											
		VECCS	VECCS/ VEXP	VBS	VBS/ VEXP	VACI	VACI/ VEXP	VCSA	VCSA/ VEXP	VEC	VEC/ VEXP	VFIP	VFIP/ VEXP
S1-25	205.4	202.3	0.98	216.1	1.05	190.0	0.93	229.1	1.12	212.2	1.03	197.0	0.96
S2-25	259.8	202.3	0.78	244.6	0.94	190.0	0.73	229.1	0.88	239.9	0.92	245.0	0.94
S3-25	293.3	202.3	0.69	295.9	1.01	190.0	0.65	229.1	0.78	290.2	0.99	285.0	0.97
S4-25	262.5	202.3	0.77	216.2	0.82	190.0	0.72	229.1	0.87	212.2	0.81	197.0	0.75
S5-25	282.2	202.3	0.72	244.6	0.87	190.0	0.67	229.1	0.81	239.9	0.85	197.0	0.70
S6-25	290.9	202.3	0.70	295.9	1.02	190.0	0.65	229.1	0.79	290.2	1.00	197.0	0.68
S7-25	299.3	202.3	0.68	388.6	1.30	286.4	0.96	343.7	1.15	406.7	1.36	298.0	0.99
S8-25	325.8	202.3	0.62	460.6	1.41	286.4	0.88	343.7	1.05	520.1	1.60	298.0	0.91
S9-25	344.7	202.3	0.59	568.6	1.65	286.4	0.83	343.7	1.00	551.2	1.60	298.0	0.86
S10-25	305.2	202.3	0.66	388.6	1.27	286.4	0.94	343.7	1.13	406.7	1.33	298.0	0.97
S11-25	338.3	202.3	0.60	460.6	1.36	286.4	0.85	343.7	1.02	520.1	1.54	298.0	0.88
S12-25	359.3	202.3	0.6	568.6	1.6	286.4	0.8	343.7	1.0	551.2	1.5	298.0	0.83
Mean value			0.70		1.19		0.80		0.96		1.21		0.87
S.D.			0.11		0.28		0.11		0.13		0.31		0.109
C.O.V			16.38		23.28		14.10		13.94		25.44		9.19



from tests on slabs specimens of similar flexural reinforcement. The experimental results were used to examine the applicability of the punching shear strength formulae given in design codes. The code provisions investigated are ECCS-203 [33], BS-8110 [34], ACI-318 [7], CSA A23.3 [21], EC2, [14] and FIP-2010 [35]. Commonly, the codes define the design punching load as the product of the design shear strength of concrete and the area of a chosen critical section of punching. Depending on the code used, the critical section for checking punching shear in slabs is located between the column face up to 2.0 times the effective slab depth. Table 2 shows a comparison between the experimental and the codes predicted ultimate loads for the test slabs.

Table 2 indicates a significant variation in the punching shear predictions from code provisions to another. The mean predicted-to-experimental ultimate load is shown to range from 0.70 to 1.21 with a coefficient of variation (C.O.V) ranging from 13.9 to 25.4%. The adequacy of the predictions is dependent mainly on the method of load application. As such, the code predictions for specimens with or without shear reinforcement, the adopted contribution of flexural reinforcement.

For test slabs without shear reinforcement in Series A and B, the superlative predictions were obtained following the BS, EC2 and FIP-2010 provisions. Otherwise, it should be noted that BS predictions slightly overestimated two slab specimens and EC2 predictions slightly overestimated only one slab specimen. The CSA provisions resulted in acceptable predictions of the ultimate load. On the other hand, the ECCS and ACI codes results are shown to be conservative. The conservative predictions of ECCS, ACI and FIP-2010 provisions attributed to that these code provisions neglected the effect of flexural reinforcement on punching shear capacity. CSA code results were the closest even with negligible effect of flexural reinforcement. The reason for this behavior may be the higher punching shears strength of concrete adopted in CSA code. That response may lead to overestimated punching shear capacity for slabs with low flexural reinforcement ratio as revealed in specimen S1-25.

For slabs with shear reinforcement the superlative predictions were obtained following the CSA provisions. ECCS code provisions predicted a very conservative punching capacity for test slabs. The

underestimated predictions of ECCS attributed to effect of shear reinforcement neglected. On the other hand, BS and EC2 code provisions resulted in unsafe predictions for all slabs with shear reinforcement. The overestimated predictions for punching capacity due to the BS and EC2 code provisions has no limits for shear reinforcement contribution as adopted in ACI, CSA and FIP-2010 provisions.

In conclusion, most of code provisions need to be refined to account the main parameters affecting the punching shear strength of flat slab. According to the comparative study above, the main parameters affecting punching shear should be revised for more accurate predictions of punching shear capacity were the shear reinforcement contribution and flexural reinforcement ratio. ECCS code provision should be refined to account the two parameters. ACI and CSA code provision should be revised to add the effect of flexural steel ratio. BS and EC2 overestimated the contribution of shear reinforcement and should be modify the limitation of maximum capacity of slabs provided with shear reinforcement.

5 Conclusions

According to this study, the following main conclusions can be drawn.

1. Flexural reinforcement ratio especially in tension side had a noticeable effect on the mode of failure and ultimate punching capacity of flat slabs.
2. Flexural reinforcement ratio and shear reinforcement had insignificant effect on the cracking loads of the test specimens, with a noticeable effect on the cracking patterns and ductility.
3. The ultimate load of test specimens increased as the tensile reinforcement increased. The enhancement in the ultimate loads due to increasing tensile reinforcement ratio was ranging between 26.0 and 42.0%.
4. Slightly enhancement (up to 12%) in ultimate loads was observed as a result of increasing compressive steel ratio.
5. Provision of shear reinforcement was shown to increase the perimeter of the failure. Specimens with shear reinforcement failed at larger perimeters than slabs without shear reinforcement.



6. The ultimate loads were increased with the addition of single leg stirrups as shear reinforcement particularly in case of radial arrangement of shear reinforcement. An increase in the ultimate load ranging between 6 and 27% was recorded for specimens with shear reinforcement compared to test slabs without shear reinforcement.
7. To the range of the test parameters investigated, the application of non-linear finite element analysis using ANSYS 10.0 package yielded satisfactory load-carrying capacities and load–deflection responses with acceptable cracking loads.
8. Codes comparison indicates a significant variation in the punching shear predictions from code to another. The ECCS shows the most conservative prediction for punching shear capacity specially in case of using shear reinforcement as the code provisions neglect the effect of shear reinforcement. The mean predicted-to-experimental ultimate load is shown to be 0.7. The predictions following the ACI, CSA and FIP-2010 are closet to the experimental results. The mean predicted-to-experimental ultimate load is shown to be 0.8, 0.96 and 0.87 for ACI, CSA and FIP-2010 respectively.

Compliance with ethical standards

Conflict of interest The authors declare that they have no conflict of interest.

References

1. Einpaul J, Ospina CE, Ruiz MF, Muttoni A (2016) punching shear capacity of continuous slabs. *ACI Struct J* 113(4):861–872
2. Al-Gasham TS, Mhalhal JM, Jabir HA (2019) Improving punching behavior of interior voided slab-column connections using steel sheets. *Eng Struct* 199:1–15
3. Liberatia EAP, Marquesa MG, Luiz L, Trautweina LM (2019) Failure analysis of punching in reinforced concrete flat slabs with openings adjacent to the column. *Eng Struct* 182:331–343
4. Torabian A, Isufi B, Mostofinejad D, Ramos AP (2019) Behavior of thin lightly reinforced flat slabs under concentric loading. *Eng Struct* 196:1–16
5. Ferreira MP, Melo GS, Regan PE, Vollum RL (2014) Punching of reinforced concrete flat slabs with double-headed shear reinforcement. *ACI Struct J* 111(2):363–374
6. Trautwein LM, Bittencourt TN, Gomes RB, Bella JCD (2011) Punching strength of flat slabs with unbraced shear reinforcement. *ACI Struct J* 108(2):197–205
7. ACI Committee 318 (2014) Building code requirements for reinforced concrete (ACI 318-14) and commentary (ACI 318R-14). American Concrete Institute, Farmington Hills
8. Yang JM, Young SY, Cook WD, Mitchell D (2010) Influence punching tests of slabs with low reinforcement ratios. *ACI Struct J* 107(4):468–475
9. Gardner NJ (1990) Punching shear of continuous flat reinforced concrete slabs. In: Annual conference of the Canadian society for civil engineering, Ottawa, ON, Canada, pp 247–256
10. Marzouk H, Hussein A (1991) Experimental investigation on the behavior of high-strength concrete slabs. *ACI Struct J* 88(6):701–713
11. Marzouk H, Hussein A (1991) Punching shear analysis of reinforced high-strength concrete slabs. *Can J Civ Eng* 18(4):954–963
12. Ramdane KE (1996) Punching shear of high performance concrete slabs. In: 4th international symposium on utilization of high-strength/high-performance concrete. Paris, pp 1015–1026
13. Guandalini S, Burdet O, Muttoni A (2009) Influence punching tests of slabs with low reinforcement ratios. *ACI Struct J* 106(1):87–95
14. BS EN 1992-1-1 (2004) Eurocode 2: design of concrete structures. General rules and rules for buildings (incorporating corrigendum January 2008, November 2010 and February 2014)
15. Birkle G, Dilger WH (2008) Influence of slab thickness on punching shear strength. *ACI Struct J* 105(2):180–188
16. Stein T, Ghali A, Dilger W (2007) Distinction between punching and flexural failure modes of flat plates. *ACI Struct J* 104(3):357–365
17. Yaser AY (2004) Behavior of high strength reinforced concrete slabs under concentrated and line loads, Ph.D Thesis, Cairo Faculty of Engineering, Cairo University, Egypt
18. Marzouk H, Eman M, Hilal MS (1998) Effect of high-strength concrete slabs on the behavior of slab-column connections. *ACI Struct J* 95(3):227–237
19. Menetrey P (1998) Relationships between flexural and punching failure. *ACI Struct J* 95(4):412–419
20. Kruger G, Burdet O, Favre R (1998) Punching tests on RC flat slabs with eccentric loading. In: 2nd International Ph.D. symposium in civil engineering. Budapest
21. CSA A23.3 (2004) Design of concrete structures for buildings (CSA A23.3-04), Canadian Standards Association. Mississauga, ON, Canada
22. Hammill N, Ghali A (1994) Punching shear resistance of corner slab-column connections. *ACI Struct J* 91(6):697–705
23. Yamada T, Nanni A, Endo K (1991) Punching shear resistance of flat slabs: influence of reinforcement type and ratio. *ACI Struct J* 88(4):555–563
24. Zaghoul A (2002) Behaviour and strength of CFRP reinforced flat plate interior column connections subjected to shear and unbalanced moments, Master thesis, Department of Civil and Environmental Engineering, Carleton University, Ottawa
25. Theodorakopoulos DD, Swamy N (2007) Analytical model to predict punching shear strength of FRP-reinforced concrete flat slabs. *ACI Struct J* 104(3):257–266



26. Theodorakopoulos DD, Swamy N (1993) Contribution of steel fibers to the strength characteristics of lightweight concrete slab–column connections falling in punching shear. *ACI Struct J* 90(4):342–355
27. Nguyen ML, Rovank M, Tran TQ, Nguyen KK, (2011) Punching shear resistance of steel fiber reinforced concrete flat slabs. In: *The twelfth east Asia-Pacific conference on structural engineering and construction*, pp 1830–1837
28. Alexander SDB, Simmonds SH (1992) Bond model for concentric punching shear. *ACI Struct J* 89(3):325–334
29. Hallgren M, Kinnunen S (1996) Increase of punching shear capacity by using high-strength concrete. In: *4th international symposium on utilization of high-strength/high-performance concrete*, Paris, pp 1015–1026
30. Gardner NJ, Shao XY (1996) Punching shear of continuous flat reinforced concrete slabs. *ACI Struct J* 93(2):219–228
31. Hallgren M, Kinnunen S (1998) Punching shear tests on column footings, Swedish National Road Administration
32. Peek R (1989) Evaluation of ductility of structures and structural assemblages from laboratory testing. In: *Bulletin of the New Zealand National Society for Earthquake Engineering*, vol 22, no 3
33. ECCS-203 (2018) Egyptian code for design and construction of reinforced concrete structures. Housing and Building Research Center, Egypt
34. British Standards Institution (1997) Structural use of concrete, BS8110: part 1-code of practice for design and construction
35. FIP Model Code for Concrete Structures (2010)

Publisher's Note Springer Nature remains neutral with regard to jurisdictional claims in published maps and institutional affiliations.

